PAPER

Overview of plasma rotation studies on the TCABR tokamak

IOP Publishing Plasma Physics and Controlled Fusion

Plasma Phys. Control. Fusion **63** (2021) 075001 (14pp) https://doi.org/10.1088/1361-6587/abf955

Overview of plasma rotation studies on the TCABR tokamak

J H F Severo[1,*], G P Canal[1], G Ronchi[1], N B Andrade[1], T Fernandes[1], M Y Ikeda[1], M P Collares[2], R M O Galvão[1], I C Nascimento[1] and M Tendler[3]

[1] Institute of Physics, University of São Paulo, São Paulo, 05508-090 SP, Brazil
[2] Federal University of Rio Grande, Rio Grande, 96203-900 RS, Brazil
[3] Alfvén Laboratory, Royal Institute of Technology, Stockholm 10044 SE, Sweden

E-mail: jhsevero@if.usp.br

Received 19 January 2021, revised 3 April 2021
Accepted for publication 19 April 2021
Published 14 May 2021

Abstract

An overview of intrinsic plasma rotation studies in Ohmic L-mode discharges carried out in the Tokamak Chauffage Alfvén Brésilien (TCABR) tokamak is presented. Measurements of plasma poloidal and toroidal rotation, and a comparison against neoclassical theory, are presented. The results show that poloidal rotation is in good agreement with neoclassical theory while toroidal rotation is found to be anomalous. A new technique that allows for high temporal resolution measurements of plasma rotation is presented. This technique is used to test two models of intrinsic toroidal rotation: the so-called Helander model (Helander *et al* 2003 *Physics of Plasmas* **10** 4396) and Rozhansky model (Rozhansky 2013 Perpendicular currents and electric fields in fully and partially ionized magnetized plasma *Physics of Plasmas* **24** 101614). As TCABR is a relatively small device, the influence of the neutrals that form the basis of this model is expected to be enhanced. The results indicate that the mechanism proposed by Helander does not contribute significantly to the intrinsic toroidal rotation in TCABR plasmas. The measurements, however, indicate that the frictional force proposed by Rozhansky might be responsible for part of the intrinsic toroidal rotation observed in TCABR plasmas.

Keywords: plasma physics and controlled fusion, spectroscopy, plasma rotation

(Some figures may appear in colour only in the online journal)

1. Introduction

According to neoclassic theory, the radial (normal to flux surface) component of the electric field, E_r, is expected to play a significant role in the transport in high temperature, low collisionality tokamak plasmas. In early studies, the relation between plasma confinement and E_r was investigated via measurements of the electric potential distribution [1, 2] and also via spectroscopic measurements of plasma rotation [3]. Since no significant effect of E_r on plasma, confinement was observed, little attention was given to it. However, after the discovery of the so-called high confinement mode (H-mode) of operation [4], which is believed to be caused by a spontaneous bifurcation of the radial electric field, the need for accurate measurements of E_r, and, consequently, plasma rotation became necessary. Nowadays, several studies have shown that plasma rotation plays an important role in the performance of tokamak plasmas [5–10]. Several benefits associated to the plasma rotation have been routinely observed in present-day tokamaks, such as reduction of growth rates of certain magnetohydrodynamic (MHD) modes [11–13], or their complete stabilization depending on the plasma conditions, and improvements on plasma confinement through the suppression of turbulence via the $\boldsymbol{E} \times \boldsymbol{B}$ shear rate [14, 15]. In the present day tokamaks, neutral beam injection (NBI) has been used to attain the benefits associated with large plasma toroidal rotation. In reactor-size machines such as ITER, however, the

* Author to whom any correspondence should be addressed.

moment of inertia of the plasma will be significantly larger. Extrapolations of experimental data from existing machines to ITER indicate that external momentum (torque) injection through NBI (about 33 N·m [16]), in addition to the intrinsic rotation, will not cause the plasma to rotate fast enough toroidally to ensure attaining the associated benefits aforementioned. Here, by intrinsic rotation is meant the one that arises when no external momentum is injected into the plasma. Therefore, predicting how the intrinsic rotation in ITER will depend on particular discharge features, such as the direction of neutral gas injection, is a quite a relevant issue. In principle, theoretical models of momentum transport and sources, validated in present-day tokamaks should be enough to provide meaningful predictions of intrinsic rotation in ITER plasmas. However, the theoretical understanding of the various relevant mechanisms are not yet sufficiently mature to provide reliable predictions. The difficulties arise mainly from the complexity of the various existing sources of intrinsic torque, such as transfer of momentum to the edge via ion orbit loss, residual stress, magnetic field ripple, among other effects. The lack of understanding is also, in part, related to the difficulty of performing accurate measurements of plasma rotation, especially in the poloidal direction [5–10].

There are many examples of the accurate predictions of the neoclassical theory for the poloidal rotation, in particular, in standard tokamak discharges [17–19]. However, there are examples of poor agreement, especially in discharges with internal transport barriers and other non-standard characteristics [20–23]. There are also examples in which the measurements are just partially explained by neoclassical theory [24–26]. Furthermore, neoclassical theory typically fails in predicting plasma rotation in the toroidal direction. A comparison between toroidal rotation measurements from different machines shows that, not only the rotation speed can be significantly different, but also the direction of the intrinsic rotation, table 1. Note, however, that toroidal rotation reversal has been observed in several machines during plasma density scans—see [9, 27–29] including references in [9]. Table 1 shows the intrinsic toroidal rotation in the plasma core of different tokamaks. In the Tokamak Chauffage Alfvén Brésilien (TCABR) tokamak, toroidal rotation measurements taken during limited Ohmic L-mode plasmas show that, as observed in other tokamaks [30–32], the plasma core rotates in the counter-current direction, while the plasma edge rotates in the co-current direction [33]. The measured toroidal rotation in the plasma core is approximately 20 km s^{-1} and is in reasonable agreement with the model proposed in [34].

In this work, an overview of intrinsic plasma rotation studies carried out on the TCABR tokamak is presented. Although TCABR is a small device, the results obtained in this tokamak give an integrated and comprehensive view of plasma rotation behavior in discharges with a poloidal limiter and in the collisional regime. Therefore, these measurements provide an important baseline for comparisons with other machines and also for modeling studies as shown in [33, 45, 50, 51]. This overview is organized as follows: in section 2, the main parameters of the TCABR tokamak are given. In section 3, poloidal rotation measurements are compared with neoclassical theory predictions. In section 4, a new technique that allows for high temporal resolution measurements of plasma rotation is presented. Toroidal rotation measurements obtained with this technique are compared with predictions from the Helander and Rozhansky models. The results are summarized in section 5.

2. The TCABR tokamak

The measurements of plasma poloidal and toroidal rotation of carbon impurities presented in this work were carried out in the TCABR tokamak. TCABR is a small size tokamak with major radius $R_0 = 0.61$ m, plasma minor radius $a = 0.18$ m, and maximum discharge duration of 100 ms. The measurements were taken during Ohmic discharges of circular cross section, in the low confinement mode (L-mode), limited by a poloidal limiter made of graphite, and in the collisional (Pfirsch-Schlüter) transport regime. The global plasma parameters in these discharges were: $a = (0.18 \pm 0.01)$ m, edge safety factor $q_{\rm edge} = (4.1 \pm 0.5)$, Ohmic heating power $P_{\rm Oh} = (230 \pm 50)$ kW, plasma current $I_{\rm p} = (90 \pm 15)$ kA and toroidal magnetic field, measured at R_0, $B_0 = (1.1 \pm 0.05)$ T. Radial profiles of electron temperature, $T_{\rm e}$, and density, $n_{\rm e}$, were measured using a Thomson scattering system [52] and C^{5+} carbon impurity temperature, $T_{\rm I}$, and density, $n_{\rm I}$, were measured via spectroscopy. Rotation velocity in both poloidal, $V_{{\rm I},\theta}$, and toroidal, $V_{{\rm I},\phi}$ directions were also measured via spectroscopy [53]. The effective ion charge was measured during typical TCABR discharges using the excitation of global Alfvén modes [54], by an external antenna, and was found to be $Z_{\rm eff} \approx 3$.

3. Plasma poloidal rotation studies

3.1. General background

Neoclassical transport theory predicts that magnetically confined plasmas in toroidal geometry must rotate in both poloidal and toroidal directions with velocities approximately given by $k_{\rm B}T_{\rm i}/eB_\phi a$ ($\lesssim 10$ km s^{-1}) in the poloidal direction and $k_{\rm B}T_{\rm i}/eB_\theta a$ ($10 - 100$ km s^{-1}) in the toroidal direction. Neoclassical plasma poloidal rotation can be estimated from the flux surface average of the plasma parallel momentum balance equation, i.e.

$$\left\langle m_i\, n\, \boldsymbol{B}\cdot\left[\frac{\partial \boldsymbol{u}}{\partial t} + (\boldsymbol{u}\cdot\boldsymbol{\nabla})\,\boldsymbol{u}\right]\right\rangle = \langle \boldsymbol{B}\cdot(\boldsymbol{J}\times\boldsymbol{B})\rangle - \langle \boldsymbol{B}\cdot\boldsymbol{\nabla}p\rangle - \langle \boldsymbol{B}\cdot(\boldsymbol{\nabla}\cdot\boldsymbol{\Pi})\rangle\,. \quad (1)$$

Here, m_i is the main ion mass, n is the plasma density, p is the total plasma pressure, $\boldsymbol{J}$ is the plasma current density, $\boldsymbol{\Pi}$ is the plasma stress tensor and $\langle\rangle$ denotes flux surface average. Rosenbluth, Hazeltine, and Hinton were the first to work out this equation to provide an expression for the steady-state, neoclassical plasma poloidal rotation velocity [55–57],

Table 1. Intrinsic toroidal rotation, in km s^{-1}, in the plasma core of different tokamaks. Positive values correspond to the co-current rotation. Dataset extracted from [35] and extended.

Machine	$u_{I,\phi}$	R_0 (m)	a (m)	B_0 (T)	I_P (kA)	Refs
LT-3	$+5$	0.4	0.1	1.0	33	[3]
PLT	-15	1.32	0.4	3.0	600	[36]
JFT-2	-13	0.9	0.25	1.8	230	[37]
Torus 2	$+16$	0.3	0.2	0.67	250	[38]
PDX	$\lesssim 3$	1.40	0.45	2.5	600	[39]
TM-4	-7	0.53	0.085	1.5	25	[40]
ISX	≈ 0	0.92	0.26	1.8	220	[41]
DIII-D	-25	1.6	0.56	2.2	2000	[42]
JET	-24	2.96	1.25	2.7	2500	[43]
TCA	$-40+40$	0.61	0.18	1.5	100	[44]
TCABR	-20	0.61	0.18	1.1	100	[45]
Alcator C-Mod	-60	0.68	0.22	5.4	800	[46]
TCV	-40	0.88	0.25	1.44	180	[47]
Tore Supra	-25	2.5	0.50	3.6	1000	[48]
Aditya-U	$-20+15$	0.75	0.25	1.0	100	[49]

$$V_{i,\theta}^{\rm neo} = \frac{k_\nu F(\psi) B_\theta}{e\, Z_i \langle B^2 \rangle} \frac{dT_i}{d\psi}. \tag{2}$$

Here, $F(\psi) = RB_\phi$, with B_ϕ being the toroidal component of the equilibrium magnetic field, and k_ν is an adimensional parameter that depends on the transport regime: $k_\nu = -2.1$ for the Pfirsch-Schlüter regime, $k_\nu = -0.5$ for the plateau regime and $k_\nu = 1.17$ for the banana regime. The main result of this theory is that the neoclassical poloidal rotation of the main ion, $V_{i,\theta}^{\rm neo}$, is proportional to the ion temperature gradient. Subsequently, Mikhailovskii and Tsypin [58], using a kinetic approach, found a more precise value for k_ν in the Pfirsch-Schlüter regime ($k_\nu = -1.83$), which has been confirmed by other works [59, 60]. The main ion poloidal rotation, however, is expected to be different from that of impurity ions of different charge states. Since measurements of spectral lines of impurity ions are usually used to estimate the poloidal rotation of the main ions, an expression relating the rotation of these two species must be used. The rotation of the different species that compose a plasma is regulated by the radial component of the plasma internal electric field, which can be estimated from the main ion momentum balance equation [61, 62],

$$E_{\rm r} = V_{{\rm i},\phi} B_\theta - V_{i,\theta}^{\rm neo} B_\phi + \frac{R\, B_\theta}{e\, Z_{\rm i}\ n_{\rm i}} \frac{dp_i}{d\psi}, \tag{3}$$

where $Z_{\rm i}$ is the main ion charge and $n_{\rm i}$ is the ion density. Equation (3) was first used in [30] to estimate how accurate neoclassical transport theory can predict plasma rotation. The radial electric field can also be estimated from the impurity ion momentum balance equation,

$$E_{\rm r} = V_{{\rm I},\phi} B_\theta - V_{I,\theta}^{\rm neo} B_\phi + \frac{R\, B_\theta}{e\, Z_{\rm I}\ n_{\rm I}} \frac{d}{d\psi} (n_{\rm I} T_{\rm I}). \tag{4}$$

By combining equations (2), (3) and (4), and assuming that $T_{\rm I} = T_{\rm i}$ and $V_{{\rm i},\phi} = V_{{\rm I},\phi}$, an expression for the poloidal rotation of impurity ions is obtained,

$$V_{I,\theta}^{\rm neo} = -\frac{RB_\theta T_{\rm i}}{eB_\phi} \left[\frac{\partial}{\partial\psi} \ln(n_{\rm i}) - \frac{1}{Z_{\rm I}} \frac{\partial}{\partial\psi} \ln(n_{\rm I}) + \left(\frac{1}{Z_{\rm i}} - \frac{1}{Z_{\rm I}} - \frac{B_\phi^2}{\langle B^2 \rangle} \frac{k_\nu}{Z_{\rm i}} \right) \frac{\partial}{\partial\psi} \ln(T_{\rm i}) \right]. \tag{5}$$

In the following section, the neoclassical poloidal rotation of impurity ions, calculated using equation (5), will be compared with measurements obtained in the TCABR discharges.

3.2. Comparison of poloidal rotation measurements with neoclassical theory

In TCABR, the plasma rotation has been measured through the Doppler shift of the line emission of both C^{2+} and C^{5+} ions, with wavelengths $\lambda_0 = 464.74$ nm and $\lambda_0 = 529.05$ nm, respectively [33, 53]. This technique is usually quite challenging, requiring highly accurate measurements due to the small displacement of the spectral lines ($\Delta\lambda \lesssim 0.01$ nm). Figure 1 shows a schematic representation of the experimental arrangement used to measure the poloidal rotation velocity of carbon impurities. In this series of measurements, the lens located in position 1 or 2 focuses the light from the plasma column onto the optical fiber, transmits it to a second collimating lens. Between the second lens and the entrance slit, a semi-mirror is used to focus the light from the xeon lamp on the entrance slit. During the tokamak discharge, the diffraction grating is set to rotate, in order to scan both the spectral line of the carbon impurity and that from Xe lamp. If the time position of both lines and the speed of the diffraction grating are known with enough precision, then it is possible to determine the wavelength of the carbon line. To obtain the rotation speed of the diffraction grating and the number of shots necessary to measure carbon impurity velocity with an uncertainty of no more than 1 km s^{-1}, the spectral lines NeI (533.07 775 nm), NeI (534.10 938 nm), and NeI (534.32 834 nm) of the Ne calibration lamp were scanned. Once the theoretical wavelength of the spectral lines and the time interval between them are

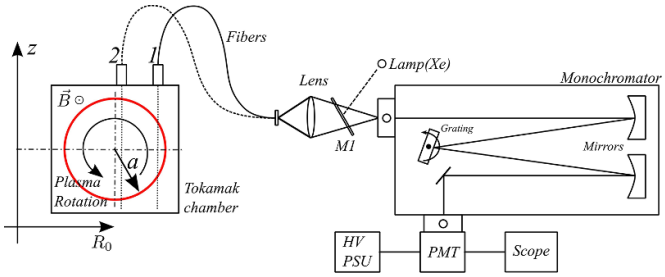

Figure 1. Schematic of the experimental setup used for poloidal rotation measurements in the TCABR tokamak. Reproduced from [53], with the permission of AIP Publishing.

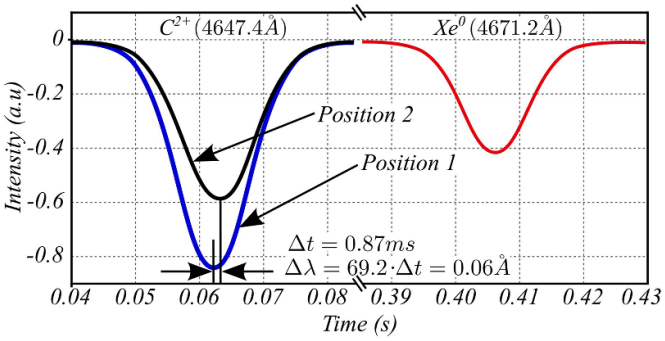

Figure 2. Temporal evolution of the C^{2+} and Xe^{0} (reference) spectral lines used to measure the Doppler shift of the C^{2+} spectral line. Reproduced from [53], with the permission of AIP Publishing.

known, it is possible to calculate the speed of the diffraction grating. The results showed that the grating rotates with a speed of 6891± 0.007 nm s^{-1}. On the other hand, to estimate the required number of shots for meaningful statistics, the wavelength of the third spectral line (534.32 834 nm) was experimentally determined from the knowledge of the rotation speed of the grating. This calibration procedure indicated that 10 shots were needed to obtain an uncertainty of 0.001 nm in the wavelength of the third line. As an example, figure 2 shows the temporal evolution of the C^{2+} and neutral xenon spectral lines, at the two vertical chords indicated in figure 1. Using this technique, it was demonstrated in [33] that the poloidal rotation in TCABR plasmas is in the electron diamagnetic direction.

The results for C^{5+} impurities are shown in figures 3(b) and (c), for the poloidal and toroidal rotation velocities. Panels (a) and (b) show the results obtained for the poloidal rotation velocity together with that predicted by the neoclassical theory, equation (5). The required electron density and temperature profiles for hydrogen and carbon were determined by Thomson scattering [52] and spectroscopy [53], respectively, and are shown in panels (d)–(f). The density profile of C^{5+} was determined from Abel inversion of line-integrated radiation measurements and scaled to the electron density profile so that it reaches a maximum of 2% of the electron density at the same radial location. In fact, the actual value of the maximum value of the C^{5+} density is not relevant to calculate the poloidal rotation velocity, since only logarithm derivatives enter in equation (5). To calculate the plasma (hydrogen) ion density profile, an effective ion charge $Z_{eff} = 3$ was assumed [54]. From quasi-neutrality, the definition of Z_{eff}, and C^{5+} measurements, the C^{6+} concentration in the plasma center was estimated, thus providing an assessment of the radial profile of the main ion density, which was required for the calculated poloidal rotation from equation (5). The equilibrium reconstruction was carried out with EFIT [63].

These results clearly indicate that, in the collisional regime of TCABR Ohmic discharges, with a graphite limiter, the value of the poloidal rotation velocity of impurity ions is rather well predicted by the neoclassical theory. The relevance of this result has been recognized by the ITER Physics Basis group [64].

The interplay between magnetic islands and plasma rotation has also been studied in TCABR. Depending on their rotation velocity, magnetic islands can interact with conducting structures outside the plasma and the machine-specific intrinsic error magnetic field. This interaction might affect the mode rotation velocity and also the plasma rotation. Furthermore, depending on their width, neighboring magnetic islands can overlap, causing stochastic regions that affect plasma rotation through the stochastic electric field. This effect, among others, makes the interplay between magnetic islands and plasma rotation an important mechanism that can contribute to the strength of intrinsic rotation. In TCABR, magnetic island rotation velocities, measured by magnetic probes, were compared with measurements of plasma rotation based on the technique described above. Analysis of the magnetic fluctuation measurements indicated the presence of a rotating $m/n = 3/1$ saturated magnetic island in the plasma edge, with poloidal rotation velocity of about 5 km s^{-1}. This value coincided with the measured plasma poloidal rotation at the mode location, i.e. at the $q = 3$ flux surface [65].

4. Plasma toroidal rotation studies

Intrinsic plasma toroidal rotation has been measured in nearly every tokamak, ranging from small devices, such as TCABR [33], to the largest machine—the Joint European Torus (JET) [43]. In small machines, intrinsic toroidal rotation can be as high as 130 km s^{-1} ([66]) while, in JET, intrinsic rotation can be as low as 30 km s^{-1} ([43]). To provide an improved understanding of how intrinsic toroidal rotation scales with plasma parameters and machine size, a simple scaling law based on theoretical arguments was constructed using data from several machines [50], including data from TCABR. This scaling suggests that the toroidal rotation in the plasma core is directly proportional to the so-called ion temperature difference and inversely proportional to the plasma current, with the constant of proportionality being about 10 km MA s^{-1} keV^{-1}. The ion temperature difference is defined as the difference between the ion temperature at the magnetic axis and that at the top of the pedestal, for H-mode plasmas, or that at the point that is closer to the separatrix, for L-mode plasmas. Interestingly, no dependence on machine size was found.

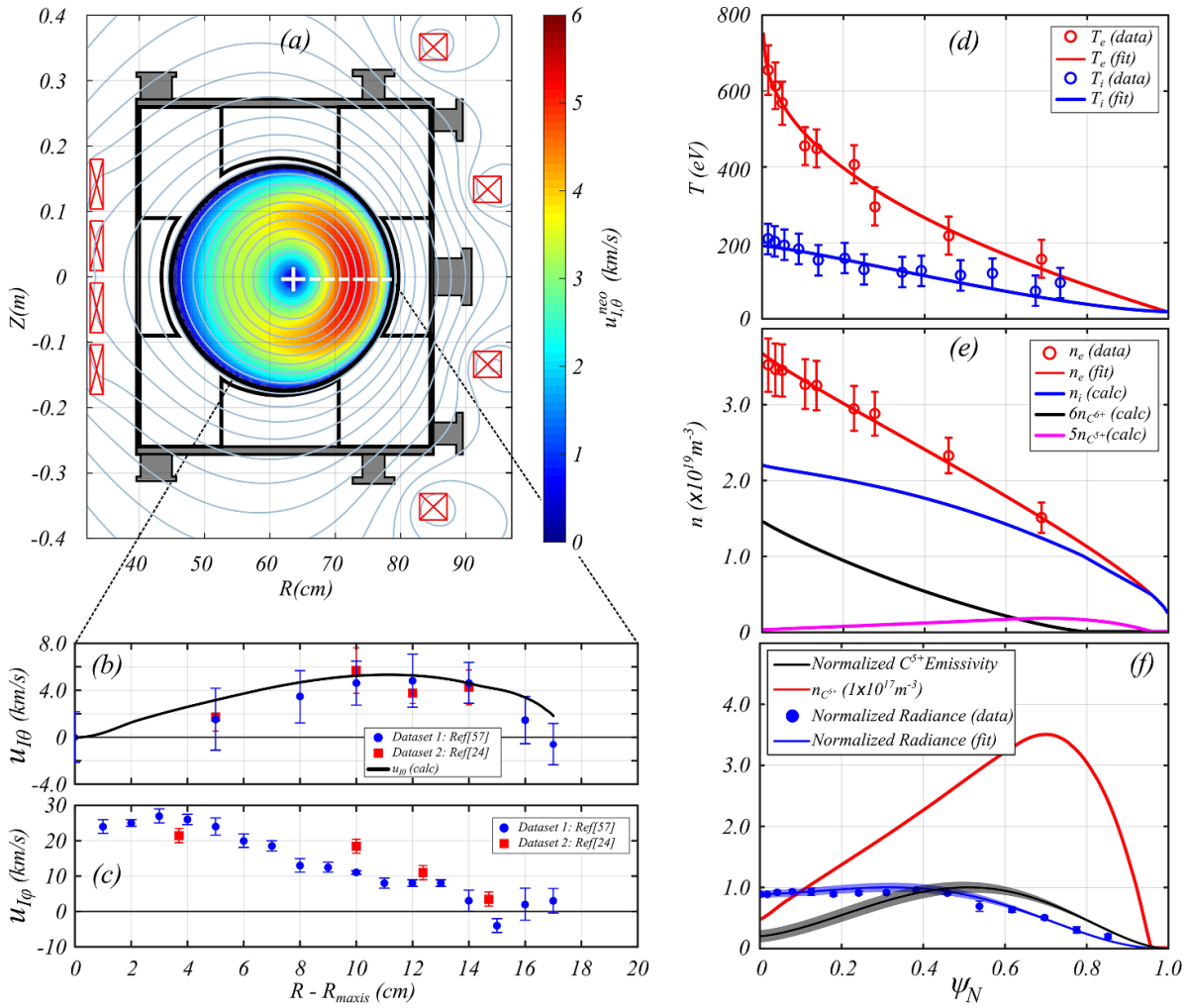

Figure 3. (a) TCABR cross-section showing the equilibrium reconstruction and the calculated poloidal rotation of C^{5+} impurity ions based on equation (5). (b) Measured and calculated radial profile, along the outboard midplane, of poloidal rotation of C^{5+} impurity ions. (c) Measured radial profile, along the outboard midplane, of toroidal rotation of C^{5+} impurity ions (positive values correspond to counter-current rotation). (d) Radial profiles of electron and C^{5+} ion temperatures. (e) Radial profiles of measured electron density and estimated hydrogen, C^{5+} and C^{6+} densities. (f) Line-integrated C^{5+} radiance, emissivity (from Abel inversion) and C^{5+} ion density.

Several models have been proposed to explain the various observations from different machines. In [67, 68], neoclassical torque was estimated for plasmas in the Pfirsch-Schlüter regime. In [69, 70], plasma viscosity due to the interaction with the neutral gas was included in a neoclassical model to explain toroidal rotation. However, since toroidal momentum is usually observed to be transported radially at rates similar to those of particles and energy, neoclassical theory alone is not expected to be enough to explain the routinely observed intrinsic toroidal rotation. In the so-called Helander model [70], the effect of a poloidally localized neutral source on plasma toroidal rotation was studied. Based on the Rozhansky works [71, 72], the influence of the direction of neutral gas injection was investigated. In the following section, intrinsic toroidal rotation measurements will be compared with predictions based on the Helander model. Also in this section, the Rozhansky model for radial currents is used to interpret the TCABR results.

4.1. Comparison of toroidal rotation measurements with Helander model

On TCABR, the model proposed by Helander was tested. This model relies on the effect of the interaction of the plasma with the neutral gas and, as TCABR is a relatively small device, the influence of neutrals and ionization sources that form the basis of this model is expected to be enhanced. These tests were carried out by using toroidal rotation measurements obtained with a new technique [45] developed at the Plasma Physics Laboratory of the University of São Paulo. This technique allows for measurements of the plasma rotation with the high temporal resolution, up to 10 kHz. The technique is based on the ratio of two different portions of the same spectral line, as represented in figure 4. The light from the plasma is collected and transmitted to a monochromator where a semi-transparent mirror is used to split the light into two beams that are directed to two different photomultipliers, as shown in figure 5.

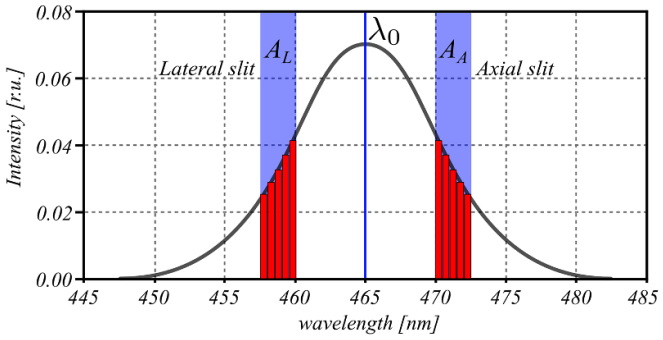

Figure 4. Schematic showing a Gaussian spectral line of C^{2+} ($\lambda_0 = 464.74$ nm) with the two regions of the spectrum, A_L and A_A, used to measure plasma rotation with a high temporal resolution. Reproduced courtesy of IAEA. Figure from [51]. Copyright 2015 IAEA.

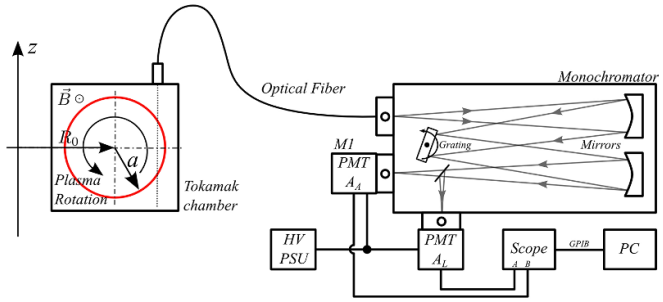

Figure 5. Experimental setup used for the high temporal resolution measurements of plasma in the TCABR tokamak. Reproduced courtesy of IAEA. Figure from [33]. Copyright 2003 IAEA.

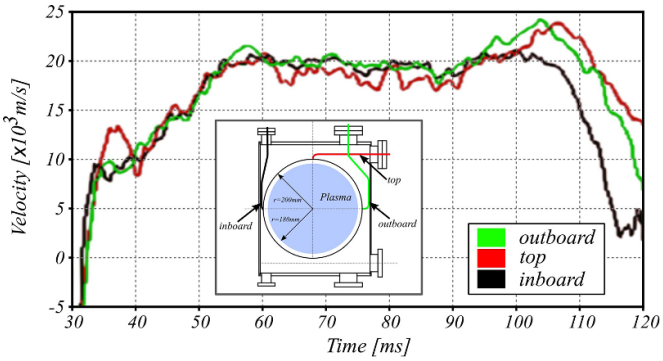

Figure 6. Temporal evolution of C^{5+} ($\lambda_0 = 529.05$ nm) toroidal rotation measured at $r = 12$ cm for three gas injection locations: outboard mid-plane (green), top (red) and inboard mid-plane (black). Insert: schematic showing the three poloidal locations used for gas puffing in TCABR. Reproduced courtesy of IAEA. Figure from [45]. Copyright 2009 IAEA.

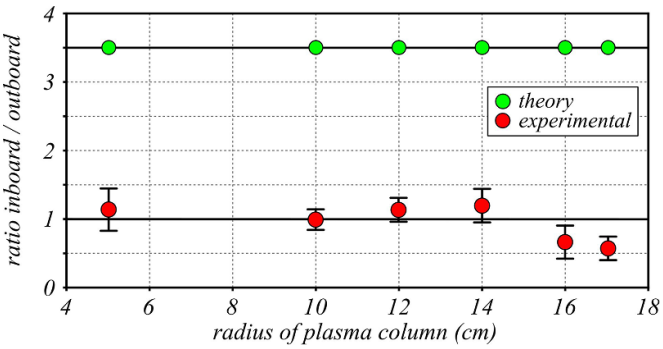

Figure 7. Ratio between toroidal rotation with inboard and outboard gas injection (red) and calculated from equation (6) (green) at different radial locations. Reproduced courtesy of IAEA. Figure from [45]. Copyright 2009 IAEA.

The lateral photomultiplier integrates the spectrum on the left of the selected spectral line (area A_L in figure 4) while the axial photomultiplier integrates the spectrum on the right of the selected spectral line (area A_A in figure 4). Therefore, as the plasma rotates, the center of the spectral line will shift and its wavelength will be displaced to the right or to the left, changing the signal ratio $R(\Delta\lambda_0) = A_L/A_A$. Here, $\Delta\lambda = \lambda - \lambda_0$ is the difference between the wavelength of the selected spectral line and the Doppler-shifted one.

Using this new technique, high temporal resolution measurements of plasma toroidal rotation were taken in TCABR [45], which allowed for testing of the Helander model. According to this model, the viscosity of the neutral gas depends not only on the plasma toroidal rotation but also on the toroidal component of the heat flux, which in turn acts as a drive for a rotation that, in the Pfirsch-Schlüter regime, is given by [70]:

$$V_{i,\phi} = \frac{2\epsilon}{eB_\theta}\frac{dT_i}{dr}\left\{f(Z_{\text{eff}})\cos(\theta) - \left[f(Z_{\text{eff}}) - 1\right]\cos(\theta_0)\right\}. \quad (6)$$

Here, $\epsilon = r/R_0$ is the plasma inverse aspect ratio, θ and θ_0 are the poloidal angle coordinate and the poloidal location of the neutral gas injection valve, and $f(Z_{\text{eff}}) = 5/2 - 0.7/Z_{\text{eff}}$, with $Z_{\text{eff}} = 3$. To verify the dependence of toroidal rotation on the poloidal location of the neutral gas injection, three gas injection valves were installed on TCABR at three different poloidal locations: $\theta_0 = 0$ (outboard mid-plane), $\theta_0 = \pi/2$ (top) and $\theta_0 = \pi$ (inboard mid-plane), see insert in figure 6.

According to equation (6), a change in toroidal rotation by a factor of approximately $2f(Z_{\text{eff}}) - 1 \approx 3.5$ is expected when comparing inboard to outboard gas injections. The temporal evolution of toroidal rotation at $r = 12$ cm for the three injection locations were measured and no significant change in the toroidal rotation was observed, figure 6. The ratio between toroidal rotation during inboard and outboard gas injection across the plasma radius can be seen in figure 7. The expected ratio based on equation (6) is also shown. No significant change is observed when different gas injection locations are used.

One possible explanation for the negligible influence of the gas injection location on toroidal rotation may be related to the specific limiter geometry of TCABR, which is a poloidal graphite limiter. For this geometry, recycling from the limiter might be dominating over the localized gas injection. Representing the particle flux injected by the gas valve by Γ_{injected}, the inward flux through the last closed flux surface coming from recycling at walls and limiter by Γ_{wall}, and the outward flux by Γ_{out}, an approximate condition for constant plasma density is

$$\Gamma_{\text{injected}} + \Gamma_{\text{wall}} = \Gamma_{\text{out}} = \frac{< n_{e0} > V_{\text{p}}}{\tau_{\text{p}}}. \quad (7)$$

Here, τ_{p} is the particle confinement time, $< n_{e0} >$ is the central line averaged plasma density, and V_{p} is the plasma volume. Taking $\tau_{\text{p}} = 10$ ms from previous experiments, $V_{\text{p}} = 0.4$ m^3, and $< n_{e0} >= 1.5 \times 10^{19}$ m^{-3}, one has $\Gamma_{\text{out}} = 6 \times 10^{20}$ particles/s, while the inward gas puff flux is $\Gamma_{\text{injected}} = 5 \times 10^{18}$ particles/s. Therefore $\Gamma_{\text{out}} >> \Gamma_{\text{injected}}$, so that plasma rotation at the edge is determined mainly by the contribution from the walls, Γ_{wall}. This occurs because TCABR is not prepared for wall conditioning such as baking and/or boronization, and the walls end up absorbing significant amounts of gas, which are then released during the discharge. This uncontrolled gas flow from the walls can be one and two orders of magnitude higher than the injected one, which might be hiding any dependence of the toroidal rotation on the poloidal location of gas injection. Note that, although the isotropic particle flow (particles per second) from the limiter is significantly larger than the one injected by the gas valve, the surface area of the limiter, from where the particles come out, is about three orders of magnitude larger than the gas valve aperture. In other words, the solid angle at which particles are emitted from the limiter is much larger than the one of the gas valve. This leads to an oriented/focused particle flux (particle per second per surface area) significantly larger in the case of the gas valve compared to the particle flux from the limiter. Since the effect predicted by Helander's model on toroidal rotation depends on the poloidal asymmetry of the neutral hydrogen density, it would have a smaller, or negligible, impact due to the low gas valve flow.

4.2. Comparison of toroidal rotation measurements with Rozhansky model

Although TCABR data do not show any dependence of toroidal velocity on the poloidal position of the gas injection, the plasma edge toroidal velocity is found to be quite sensitive to density variations, figure 8.

Toroidal rotation measurements at $r = 17$ cm during a discharge in which the plasma density was increased through a pre-programmed gas puffing using radial injection show that, regardless of the poloidal location of gas injection, an increase in plasma edge toroidal rotation is observed. Note that the time trace of the voltage that controls the gas injection valve was programmed to cause the rotation to return to about its value just before the injection.

To further investigate this apparent source of toroidal momentum in the plasma edge, a series of experiments, designed based on the Rozhansky work [51], was carried out on TCABR.

According to the model proposed by Rozhansky, a frictional force acting on particle species j due to interaction with particle species k, $\boldsymbol{R}_{j,k}$, causes the j-species to drift in the $\boldsymbol{R}_{j,k} \times \boldsymbol{B}$ direction. Assuming the injected neutral (H_2) gas is at room temperature, its average velocity is about 1.6 km s^{-1}, while the edge toroidal rotation velocity is about 3.0 km s^{-1} for radial gas injection, figure 9.

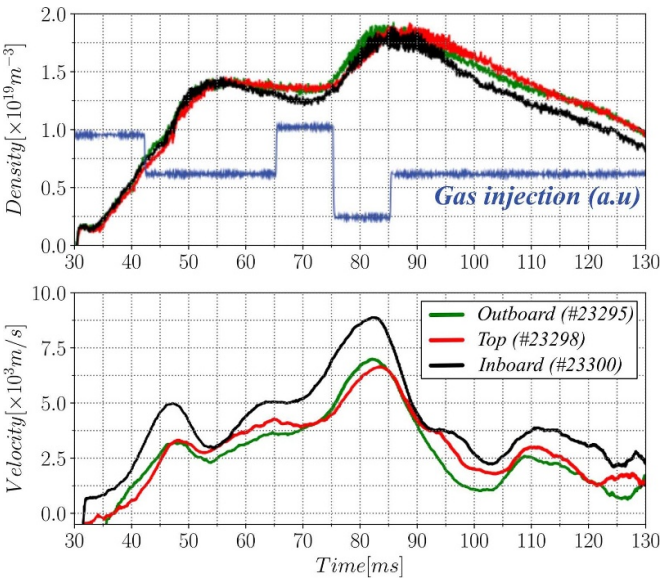

Figure 8. Temporal evolution of the plasma density (top panel) and intrinsic toroidal rotation of C^{2+} ($\lambda_0 = 464.74$ nm) at $r = 17$ cm (bottom panel) for three gas injection locations. Uncertainties are about 1.8 km s^{-1}.

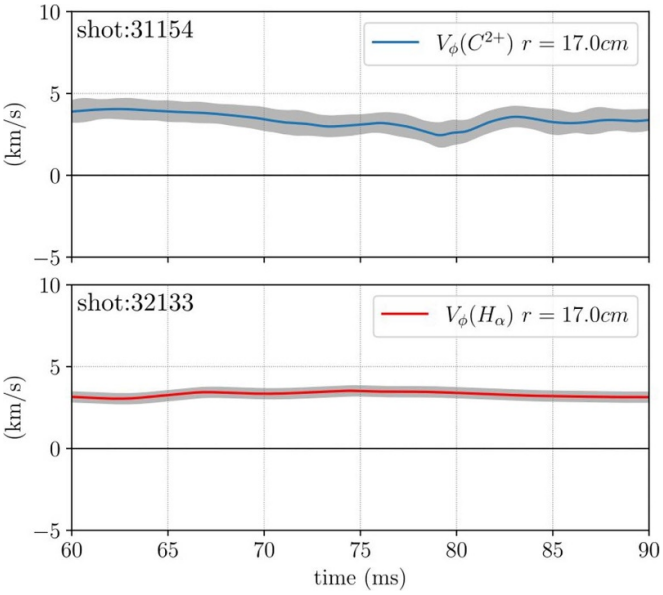

Figure 9. Toroidal rotation velocity of (top) C^{2+} and (bottom) neutral hydrogen species at $r = 17$ cm using radial gas injection. Uncertainties are show for both measurement, namely 1.8 km s^{-1} for C^{2+} and 0.6 km s^{-1} for neutral hydrogen.

For a counter injection, the frictional force due to collisions between ions and neutral atoms is maximum and therefore the $\boldsymbol{R}_{\mathbf{I},\mathbf{H}_0} \times \boldsymbol{B}$ drift velocity should be higher. This velocity in turn produces a current in the radial direction that must accelerate the plasma in the toroidal direction. In figure 10 is shown the frictional force R_{ϕ,i,H_0} between the neutral particles and the ions, the drift velocity $V_{r,d}$ resulting from this frictional force, the radial current J_r resulting from the drift of the ions, and the force F_ϕ resulting from the cross product of the radial current

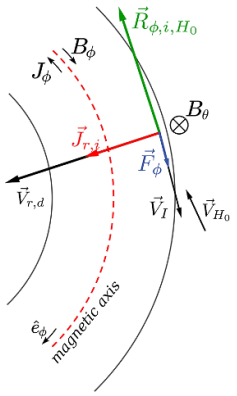

Figure 10. Schematic showing the drift velocity $V_{r,d}$ in black, radial current J_r in red and resulting force in the toroidal direction F_ϕ in green, all due to the frictional force R_{ϕ,i,H_0} between ions and neutral particles in $-\phi$ direction.

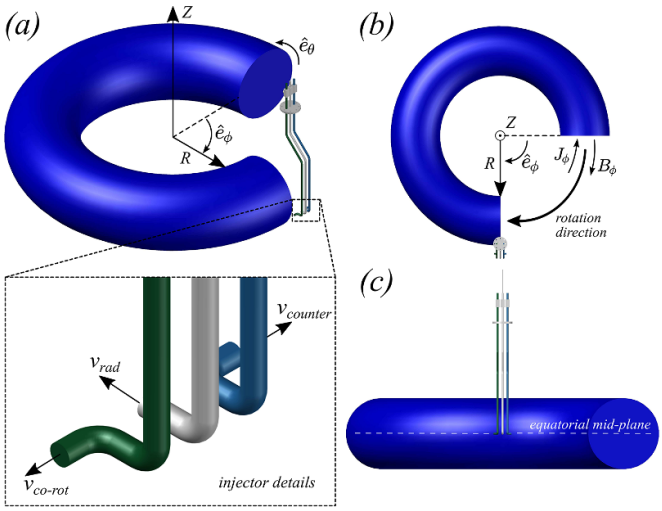

Figure 11. Schematic showing a TCABR gas injection system, which is composed of three gas injection valves. This system was installed at the top of TCABR. The injection point is at the outboard midplane and injection angles are $+70^\circ$, 0° and -70°, all viewed from the top. Here, $\pm 90^\circ$ corresponds to injection tangent to the plasma surface and 0° correspond to purely radial injection.

with the poloidal magnetic field. By assuming an electron temperature of 20 eV and density of $1\times\ 10^{18}\,\mathrm{m}^{-3}$ in the plasma edge, neutrals are expected to penetrate about 4 cm into the plasma, which is about the size of the region where this mechanism is expected to exist. To further investigate this mechanism, a new gas-injection system, composed by three gas injection valves, was installed at the top of TCABR, figure 11.

This system allows for gas to be injected in the radial direction as well as in the toroidal direction, either in co- or counter-rotation. For this series of experiments, the discharge is initiated and sustained using only one of the three gas valves and no perturbative gas puff was used. The gas valve selected is used to keep the plasma density constant during the plasma rotation measurements. Also, the number of channels for measuring plasma rotation was increased to three, allowing

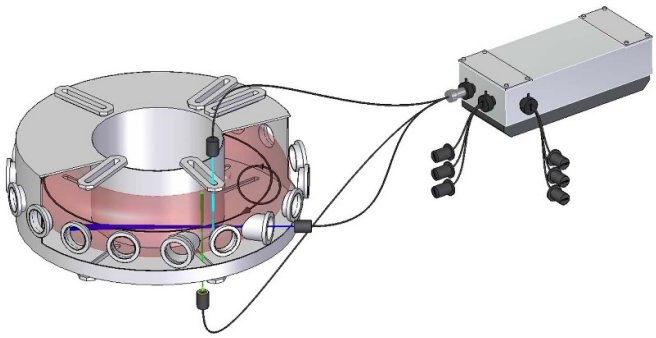

Figure 12. Experimental setup used for the temporal evolution of the poloidal and toroidal impurity rotation velocities in the TCABR tokamak. Reproduced courtesy of IAEA. Figure from [51]. Copyright 2015 IAEA.

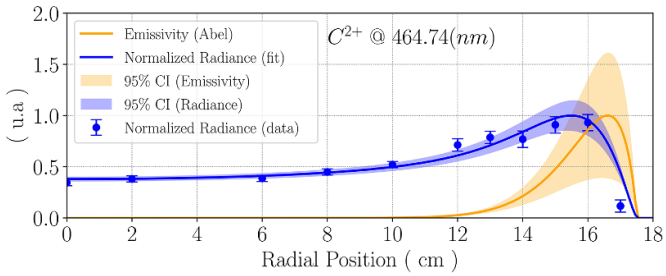

Figure 13. Measured line-integrated C^{2+} spectral line radiance and its associated emissivity obtained through Abel inversion. Both profiles were normalized to their maximum value.

for simultaneous measurements of the temporal evolution of both poloidal and toroidal rotation velocities, figure 12.

To test the influence of the direction of the gas injection on plasma rotation, three parameters were defined: $V_{\phi,\mathrm{co}}$, $V_{\phi,\mathrm{counter}}$ and $V_{\phi,\mathrm{rad}}$, which correspond to toroidal rotation velocities measured at the plasma edge ($r = 17$ cm) when the plasma discharge is carried out entirely using a gas injection in the same direction of the plasma toroidal rotation, in the opposite direction of the plasma toroidal rotation, and in the radial direction, respectively. The injection point is at the outboard midplane and injection angles are $+70^\circ$, 0° and -70°, all viewed from the top. Here, $\pm 90^\circ$ corresponds to injection tangent to the plasma surface and 0° correspond to purely radial injection. We stress that gas was injected in just one direction during the discharge, i.e. only one gas valve is used at a time to sustain the plasma density constant during the discharge. Due to fluctuations in the toroidal rotation measurements caused by changes in machine wall conditioning prior to each discharge, several discharges were carried out for improving the data statistics. Furthermore, since gas injection in the radial direction is the most frequently used for particle control in nearly every tokamak, the toroidal rotation measurements $V_{\phi,\mathrm{co}}$ and $V_{\phi,\mathrm{counter}}$ were normalized to $V_{\phi,\mathrm{rad}}$, and also the ratio $V_{\phi,\mathrm{counter}}$ / $V_{\phi,\mathrm{co}}$ was considered, all for the same spectral line. In addition, line-integrated radiance measurements and emissivity (from Abel inversion) of C^{2+}, figure 13, show that the maximum of the emissivity is localized at about $r = 16.5$ cm.

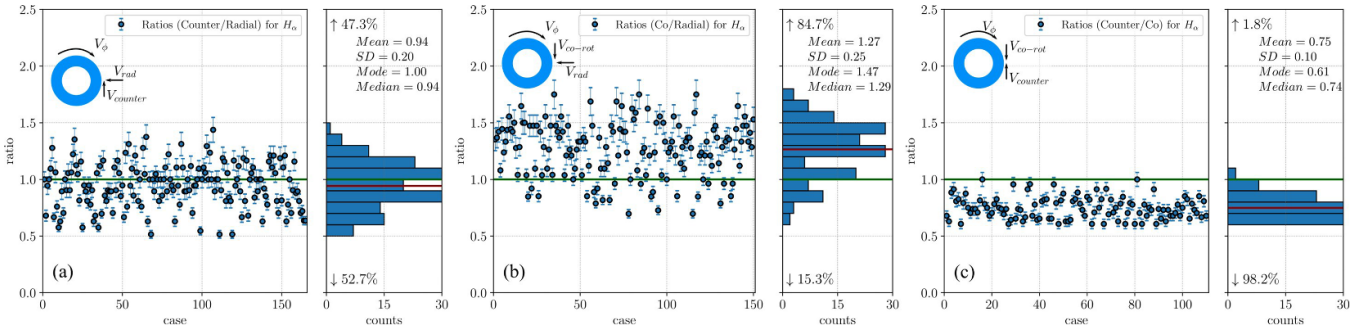

Figure 14. Ratio of the measured neutral hydrogen (H_α spectral line) toroidal rotation during (a) counter-rotation, (b) co-rotation gas injection, and (c) counter-rotation / co-rotation ratio from several discharges, both normalized to the measured neutral hydrogen (H_α spectral line) toroidal rotation during radial gas injection. The measurements were taken in the plasma edge ($r = 17$ cm).

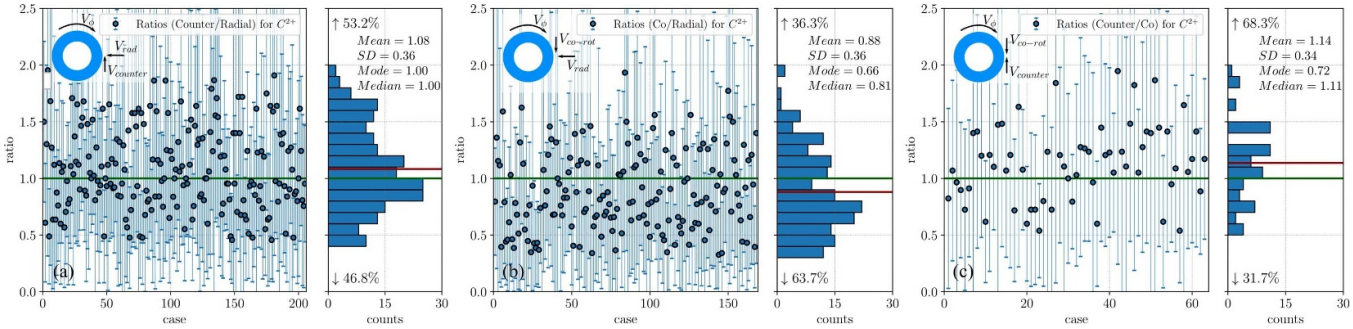

Figure 15. Ratio of the measured C^{2+} ($\lambda_0 = 464.74$ nm) toroidal rotation during (a) counter-rotation, (b) co-rotation gas injection and (c) counter-rotation / co-rotation ratio from several discharges, both normalized to the measured C^{2+} toroidal rotation during radial gas injection. The measurements were taken at the plasma edge ($r = 17$ cm).

Table 2. Velocity ratios and frequency of events calculated from the data shown in figures 14 and 15.

Velocity ratios > 1	Neutral hydrogen	C^{2+} carbon
$V_{\phi,\mathrm{co}}$ / $V_{\phi,\mathrm{rad}}$	1.27± 0.25–84.7%	0.88± 0.36–36.3%
$V_{\phi,\mathrm{counter}}$ / $V_{\phi,\mathrm{rad}}$	0.94± 0.20–47.3%	1.08± 0.36–53.2%
$V_{\phi,\mathrm{counter}}$ / $V_{\phi,\mathrm{co}}$	0.75± 0.10–1.8%	1.14± 0.34–68.3%

Consequently, the maximum of neutral hydrogen and carbon emissivities must also be very close to the limiter, which is located at $r = 18$ cm. Neutral hydrogen and C^{2+} toroidal rotation velocities were measured for these three gas injection directions. The ratios $V_{\phi,\mathrm{co}}/V_{\phi,\mathrm{rad}}$, $V_{\phi,\mathrm{counter}}/V_{\phi,\mathrm{rad}}$ and $V_{\phi,\mathrm{counter}}$ / $V_{\phi,\mathrm{co}}$ for both H_α and C^{2+} can be seen in figures 14 and 15, respectively. These results are summarized in table 2, which shows the frequency of events for velocity ratios > 1 calculated from this data set.

The results presented in table 2 show that neutral hydrogen and C^{2+} toroidal rotation velocities have significantly different responses to the gas injection direction. For neutral hydrogen atoms, the normalized toroidal rotation increases when gas is injected in the same direction of the plasma toroidal rotation and decreases when the injection is in the opposite sense, as indicated by the data presented in figure 14 and summarized in table 2.

Since for neutral hydrogen the product $\boldsymbol{R}_{\mathbf{I},\mathbf{H}_0} \times \boldsymbol{B} = 0$, this result is trivially explained by simple direct momentum transfer from the neutral hydrogen atoms to the excited ones, which are dragged along by the main plasma. For the case of C^{2+} impurity ions, unlike that of neutral gas, the product $\boldsymbol{R}_{\mathbf{I},\mathbf{H}_0} \times \boldsymbol{B} \neq 0$ and the toroidal rotation is expected to be affected by toroidal components of the frictional force between H_0 atoms and C^{2+} ions. Here, H_0 and I subscripts represent neutral hydrogen atoms and impurity ions, respectively. The frictional force is given by $\boldsymbol{R}_{\boldsymbol{I},\boldsymbol{H_0}} = -m_I n_I \nu_{I,H_0} (\boldsymbol{V_I} - \boldsymbol{V_{H_0}})$, where ν_{I,H_0} is the collision frequency between carbon ions and neutral hydrogen atoms. The results shown in figure 15, and summarized in table 2, indicate that, for H_0 co-rotation injection, i.e. injection in the sense of the main plasma rotation and opposite to the sense of the plasma current in the case of TCABR, the value of the toroidal velocity of the C^{2+} ions is smaller than the values observed for radial injection. For counter-rotation injection, on the other hand, this value is slightly higher than one but is statistically comparable to that obtained for radial injection. The ratio $V_{\phi,\mathrm{counter}}$ / $V_{\phi,\mathrm{co}}$ also confirm that of $V_{\phi,\mathrm{counter}} > V_{\phi,\mathrm{co}}$.

4.2.1. Radial current estimation. A simple model is proposed to explain the ratio between the observed values of $V_{\phi,\mathrm{counter}}$, $V_{\phi,\mathrm{co}}$ and $V_{\phi,\mathrm{rad}}$. We start from the single-fluid momentum balance equation [62].

$$\rho \frac{d\boldsymbol{u_i}}{dt} = \boldsymbol{J} \times \boldsymbol{B} - \nabla \cdot \boldsymbol{\Pi} - \nabla (p_e + p_i) - m_i n_i \nu_{i,H_0} \boldsymbol{u_i} \qquad (8)$$

where $\rho \simeq n_i m_i$ is the fluid mass density, $\boldsymbol{u_i}$ is the ion velocity, $\boldsymbol{J}$ is the current density, $\boldsymbol{\Pi}$ is the ion viscosity stress tensor, $p_{e,i}$ are the partial pressures for electrons and ions, and d/dt is the sum of the convective and time partial derivatives. We remark that this equation is written in a coordinate system where the velocity of the neutral particles is equal to zero. The surface averaged toroidal components of equation (8) can then be written as:

$$m_i n_i \frac{d\boldsymbol{V_{i,\phi}}}{dt} = \Theta \langle J_r \rangle \boldsymbol{B_0} - \left\langle (\boldsymbol{B}_\phi / \boldsymbol{B}^2) \cdot \boldsymbol{\nabla} \cdot \boldsymbol{\Pi} \right\rangle \boldsymbol{B}_0 - m_i n_i \nu_{i,H_0} \boldsymbol{V_{i,\phi}} \quad (9)$$

where $V_{i,\phi}$ is the averaged toroidal velocity in the magnetic surface, $\theta = B_\theta / B_\phi$ the ratio of the poloidal and the toroidal magnetic fields. Our interest here is to know what is the increase in toroidal velocity that can be produced by the radial current that arises due to the drift of ions that is generated by the frictional force. Therefore, we will consider only the stationary case and the convective derivative will also be neglected since the radial flow can be considered small. As can be shown, the second term on the right side of equation (9) is equal to zero when there is symmetry in the ϕ direction. In the case of the TCABR, it can also be neglected. Therefore equation (9) becomes:

$$\Theta \langle J_r \rangle \boldsymbol{B_0} = m_i n_i \nu_{i,H_0} \boldsymbol{V_{i,\phi}}. \quad (10)$$

To properly model the results of the velocity ratios, some estimates have been made and are expressed below:

4.2.2. Velocities. The average value of the toroidal speed of the C^{2+} ions were taken from the data set for co-injection ($V_i = V_I = 2.7\,\mathrm{km\ s^{-1}}$), and the injection speed of the hydrogen atoms was considered equal to the thermal speed ($V_{H_0} = 1.6\,\mathrm{km\ s^{-1}}$).

4.2.3. Density and temperature at plasma edge. For radial position $r = 17$ cm the plasma density of ions and electron was considered equals and of order $1 \times 10^{18}\ \mathrm{m^{-3}}$. The temperature of ions and electrons also equals and of order 20 eV.

4.2.4. Neutral density. The density of neutrals was estimated from the condition for constant plasma density (7).

$$\Gamma_{\mathrm{injected}} + \Gamma_{\mathrm{wall}} = \Gamma_{\mathrm{out}} = \frac{< n_{e0} > V_p}{\tau_p} = n_{H_0} V_{H_0} S = 6 \times 10^{20} \mathrm{particles\,s^{-1}} \quad (11)$$

where $\Gamma_{\mathrm{injected}}$ is injected flux through gas puff, Γ_{wall} is the inward flux coming from recycling at walls and limiter, Γ_{out} is outward flux and S is the Inner chamber area. So from (11) we estimate $n_{H_0} = 5 \times 10^{16} \mathrm{m^{-3}}$. The amount of ions N_i involved in drift can be also estimated from (11) however, now we only consider the $\Gamma_{\mathrm{injected}}$ flux generated by a gas puff. Since the TCABR tokamak discharge duration is 100 ms, approximately 10^{17} particles are injected in this time interval. Therefore, it is expected that the amount of particles that participate in the generation of current is approximately 10^{17}.

Table 3. Physical quantities used to estimate the speed ratios.

Parameter	Symbol	Estimated value
Ion mass	m_{i}	1.67×10^{-27} kg
Electron temperature ($r = 17$ cm)	T_{e}	20 eV
Ion density ($r = 17$ cm)	n_{i}	$1 \times 10^{18}\ \mathrm{m^{-3}}$
Neutral density	n_{H_0}	$5 \times 10^{16}\ \mathrm{m^{-3}}$
Poloidal magnetic field ($r = 17$ cm)	B_θ	89×10^{-3} T
Toroidal magnetic field ($r = 17$ cm)	B_ϕ	0.84 T
Toroidal magnetic field ($r = 0$ cm)	B_ϕ	1.07 T
Amount of ions involved in the current generation	n_{i_0}	1×10^{17} particles
Ion velocity	V_{i}	$2.7 \times 10^{3}\ \mathrm{m\ s^{-1}}$
Hydrogen thermal velocity	V_{H_0}	$1.6 \times 10^{3}\ \mathrm{m\ s^{-1}}$
Ion-neutral collisional frequency	ν_{i,H_0}	$2000\ \mathrm{s^{-1}}$
Charge exchange coefficient rate	$< \sigma_{\mathrm{CX}} v_i >$	$4 \times 10^{-8}\ \mathrm{cm^3\ s^{-1}}$
Ionization coefficient rate	$< \sigma_{\mathrm{ion}} v_i >$	$2 \times 10^{-8}\ \mathrm{cm^3\ s^{-1}}$
Neutral penetration	δ	4 cm

Table 4. Velocities ratios calculated from the data set showing in table 3.

Mean velocity and ratio	Estimation	Experiment
$V_{\phi,\mathrm{counter}}/V_{\phi,\mathrm{rad}}$	1.07	1.08 ± 0.36
$V_{\phi,\mathrm{co}}/V_{\phi,\mathrm{rad}}$	0.93	0.88 ± 0.36
$V_{\phi,\mathrm{counter}}/V_{\phi,\mathrm{co}}$	1.14	1.14 ± 0.34

4.2.5. Penetration of neutrals. Since in this section we are investigating the influence of gas injection on toroidal rotation, it is necessary to estimate how deep the neutral particles can penetrate in the plasma column. As was pointed out by Tendler and Reifetz [73] several reactions are important in the creation of ionized particle sources or sinks in hydrogen plasmas. The two main processes responsible for the concentration of neutral in the plasma column are ionization of the atomic and molecular hydrogen and charge exchange [73, 74]. Therefore, the penetration δ of neutral particles in the plasma column can be estimated by the mean free path of these two processes that we represent by λ_{CX} and λ_{ion}. According to [73] it can be estimated as $\delta = (\lambda_{\mathrm{CX}}.\lambda_{\mathrm{ion}}/2)^{1/2}$ where both mean free path can be evaluated from the coefficient rate for these two processes. In [75] one can find the cross sections and the coefficient rates for the main reactions that happen in hydrogen and helium plasmas. For electron temperature of $20eV$, one gets for charge exchange coefficient rate $< \sigma_{\mathrm{CX}} v_i > = 4 \times 10^{-8} < \sigma_{\mathrm{CX}} v_i > = 4 \times 10^{-8}\ \mathrm{cm^3\ s^{-1}}$ and for ionization $< \sigma_{\mathrm{ion}} v_i > = 2 \times 10^{-8}\ \mathrm{cm^3\ s^{-1}}$. Cornelis and others [76] proposes the following expression to calculate the charge exchange rate $\langle \sigma_{\mathrm{CH}} v_i \rangle\,(\mathrm{cm^3\ s^{-1}}) = 10^{-8} [T_i(\mathrm{eV})]^{0.318}$. For a temperature of 20 eV, one gets in the Cornelis' formula $2.6 \times 10^{-8}\ \mathrm{m^3\ s^{-1}}$. So, replacing the values of the mean free

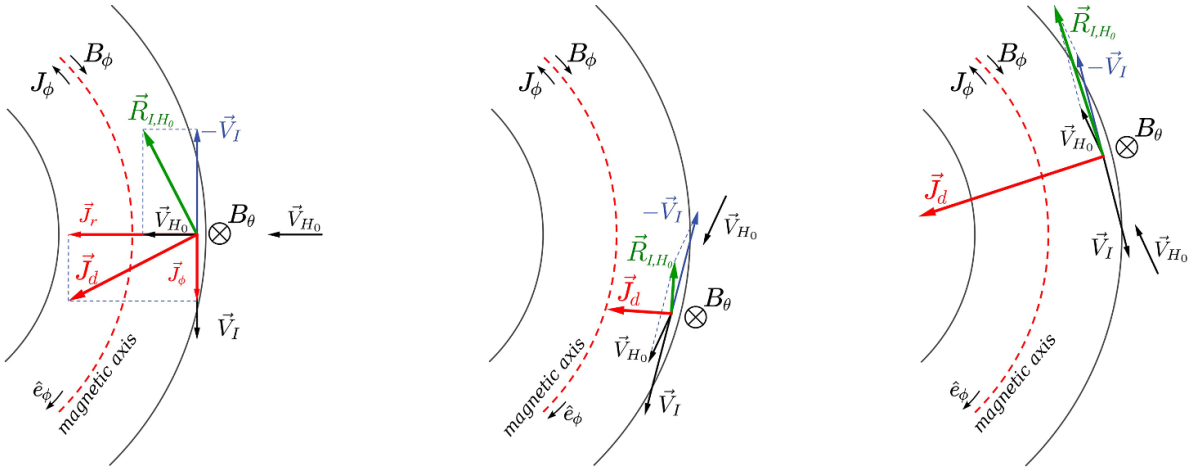

Figure 16. Schematic of the gas injection ($\boldsymbol{u}_{\mathbf{H}_0}$) and edge C^{2+} toroidal rotation ($\boldsymbol{u}_{\mathbf{I}}$) velocities, friction force ($\boldsymbol{R}_{\mathbf{I},\mathbf{H}_0}$) and the associated $\boldsymbol{R}_{\mathbf{I},\mathbf{H}_0} \times \boldsymbol{B}$ drift velocity ($\boldsymbol{u}_{\mathbf{d}}$) for the three injection directions: radial, co-rotation and counter-rotation. Injection angles are 0° and ±70°, viewed from the top, in which ±90° corresponds to injection tangent to the plasma surface and 0° correspond to purely radial injection.

path in the expression for penetration we get $\delta = 4$ cm. Therefore, considering that the gas is injected in the region close to the limited ($a = 18$ cm) and that it can penetrate up to 4 cm then in a range that goes from 18 to 12 cm, one can investigate the effect of the gas injection on rotation toroidal.

4.2.6. Ion-neutral collision frequency. To calculate the friction force, R_{i,H_0} used in our estimations we made use of the ion-neutral collision frequency $\nu_{i,H_0} = <\sigma_{CX}, v_i> n_{H_0} = 2000\ s^{-1}$.

In the tables 3 and 4 in the sequel, we summarized all values that were used in our estimations and velocity ratios respectively. Finally, in our calculations, it was considered that $V_{I,\phi} = V_{i,\phi}$

The good agreement of the experimental results with the estimated values for the velocity ratios indicates that the small increase in the toroidal rotation speed produced by the gas injection in the counter direction is a consequence of the appearance of a radial current. Current, in turn, is produced by the drift of the ions in the radial direction that arises due to the frictional force between neutral atoms and ions. To better visualize this effect, in figure 16 the three types of injection and the current that arise as a result of these injections are drawn. Since the toroidal velocity is proportional to the current, based on the module of the vector J_d, it is possible to visually verify that the ratio $V_{\phi,\text{counter}}/V_{\phi,\text{rad}} \geq 1$, $V_{\phi,\text{co}}/V_{\phi,\text{rad}} < 1$ and $V_{\phi,\text{counter}}/V_{\phi,\text{co}} > 1$, which agrees with the experimental results. The measurements presented in figure 15(a) indicate that both radial and counter rotation injection have similar effects on toroidal rotation. These expected effects are in qualitative and quantitative agreement with the observed $V_{\phi,\text{counter}}/V_{\phi,\text{rad}} > 1$ in only 53% of the cases, which means that $V_{\phi,\text{counter}} \approx V_{\phi,\text{rad}}$. The observed $V_{\phi,\text{co}}/V_{\phi,\text{rad}} < 1$ in 64% of the cases while the observed $V_{\phi,\text{counter}}/V_{\phi,\text{co}} > 1$ in 68% of the cases. In conclusion, our understanding of this process is that the frictional force produced by the ions-neutral collisions produces a drift of the ions in the radial direction that gives rise to a current in the same direction and consequently causes the speed of rotation of these ions to increase in the toroidal direction.

The good agreement of numerical values with experimental for the ratios indicates that the frictional force between plasma ions and neutral gas injected can be regarded as a source for intrinsic plasma rotation.

5. Conclusions

In this work, an overview of intrinsic plasma rotation studies performed on the TCABR tokamak is presented. The experiments presented here were carried out in Ohmic L-mode plasmas of circular cross-section, limited by a poloidal graphite limiter, and in the Pfirsch-Schlüter transport regime. The technique based on Doppler shift used for poloidal rotation measurements in TCABR was presented. Using this technique, it was shown that the poloidal rotation in TCABR plasmas is in the electron diamagnetic direction, with the measured values being in good agreement with neoclassical theory. The measurements show that the plasma poloidal rotation at the position of a $m/n = 3/1$ magnetic island coincides with the magnetic island poloidal rotation.

To better understand how intrinsic toroidal rotation scales with plasma parameters, a scaling law was constructed using data from several machines [50], including TCABR. The scaling indicates that toroidal rotation in the plasma center increases with the ion temperature difference and decreases with plasma current, with the constant of proportionality being about 10 km MA s^{-1} keV^{-1}.

A new technique that allows for high temporal resolution measurements of plasma rotation was also presented. Using this new technique, plasma toroidal rotation measurements with temporal resolutions of up to 10 kHz were carried out on TCABR [45]. This technique was used to test the Helander model. To investigate the possible dependence of toroidal

rotation on the poloidal location of injection proposed by Helander, three gas injection valves were installed on TCABR at three different poloidal locations. The measurements show no significant change in the toroidal rotation when different gas injection locations are used. One possible explanation for that might be the high recycling caused by the specific limiter geometry of TCABR, which seems to foreclose an investigation on the importance of this mechanism. The high temporal resolution technique was also used to study the influence of the direction of the gas injection on toroidal rotation. Toroidal rotation measurements suggest that the frictional force proposed in the Rozhansky works can indeed produce a drift velocity in the radial direction which in turn produces radial currents that can be regarded as a source of intrinsic plasma rotation.

Data availability statement

All data that support the findings of this study are included within the article (and any supplementary files).

Acknowledgments

This work was supported by the São Paulo Research Foundation FAPESP (procs: 2002/135366-1, 2003/11147-0 2010/50496-4, 2014/13296-8 and 2018/09734-0). This study was financed in part by the Coordenação de Aperfeiçoamento de Pessoal de Nível Superior—Brasil (CAPES)—Finance Code 001.

ORCID iDs

J H F Severo https://orcid.org/0000-0001-6271-666X
G Ronchi https://orcid.org/0000-0003-3097-3033

References

[1] Hosea J C, Jobes F C, Hickok R L and Dellis A N 1973 Rotation and structure of low-frequency oscillations inside the ST-Tokamak plasma *Phys. Rev. Lett.* **30** 839–42
[2] Razumova K A 1984 Results from t-7, t-10, t-11 and TM-4 tokamaks *Plasma Phys. Control. Fusion* **26** 37–47
[3] Bell M G 1979 Measurements of plasma rotation in tokamak LT-3 *Nucl. Fusion* **19** 33–8
[4] Wagner F *et al* 1984 Development of an edge transport barrier at the H-mode transition of ASDEX *Phys. Rev. Lett.* **53** 1453–6
[5] Ida K 1998 Experimental studies of the physical mechanism determining the radial electric field and its radial structure in a toroidal plasma *Plasma Phys. Control. Fusion* **40** 1429–88
[6] Rice J E 2008 Spontaneous rotation and momentum transport in tokamak plasmas *J. Phys.: Conf. Ser.* **123** 012003
[7] deGrassie J S 2009 Tokamak rotation sources, transport and sinks *Plasma Phys. Control. Fusion* **51** 124047
[8] Ida K and Rice J 2014 Rotation and momentum transport in tokamaks and helical systems *Nucl. Fusion* **54** 045001
[9] Rice J E 2016 Experimental observations of driven and intrinsic rotation in tokamak plasmas *Plasma Phys. Control. Fusion* **58** 083001
[10] Peeters A *et al* 2011 Overview of toroidal momentum transport *Nucl. Fusion* **51** 094027
[11] Garofalo A M *et al* 1999 Direct observation of the resistive wall mode in a tokamak and its interaction with plasma rotation *Phys. Rev. Lett.* **82** 3811–4
[12] Ozeki T and J- team 2003 Studies of MHD behaviour in JT-60u *Plasma Phys. Control. Fusion* **45** 645–55
[13] Politzer P *et al* 2008 Influence of toroidal rotation on transport and stability in hybrid scenario plasmas in DIII-d *Nucl. Fusion* **48** 075001
[14] Hahm T S and Burrell K H 1995 Flow shear induced fluctuation suppression in finite aspect ratio shaped tokamak plasma *Phys. Plasmas* **2** 1648–51
[15] Burrell K H 1997 Effects of E×B velocity shear and magnetic shear on turbulence and transport in magnetic confinement devices *Phys. Plasmas* **4** 1499–518
[16] Chrystal C, Grierson B A, Solomon W M, Tala T, deGrassie J S, Petty C C, Salmi A and Burrell K H 2017 Dependence of intrinsic torque and momentum confinement on normalized gyroradius and collisionality in the DIII-D tokamak *Phys. Plasmas* **24** 042501
[17] Field A R, McCone J, Conway N J, Dunstan M, Newton S and Wisse M 2009 Comparison of measured poloidal rotation in MAST spherical tokamak plasmas with neo-classical predictions *Plasma Phys. Control. Fusion* **51** 105002
[18] Bell R E, Andre R, Kaye S M, Kolesnikov R A, LeBlanc B P, Rewoldt G, Wang W X and Sabbagh S A 2010 Comparison of poloidal velocity measurements to neoclassical theory on the national spherical torus experiment *Phys. Plasmas* **17** 082507
[19] Bortolon A, Camenen Y, Karpushov A, Duval B, Andrebe Y, Federspiel L and Sauter O 2013 Indirect measurement of poloidal rotation using inboard–outboard asymmetry of toroidal rotation and comparison with neoclassical predictions *Nucl. Fusion* **53** 023002
[20] Bell R E, Levinton F M, Batha S H, Synakowski E J and Zarnstorff M C 1998 Poloidal rotation in TFTR reversed shear plasmas *Phys. Rev. Lett.* **81** 1429–32
[21] Crombé K *et al* 2005 Poloidal rotation dynamics, radial electric field and neoclassical theory in the jet internal-transport-barrier region *Phys. Rev. Lett.* **95** 155003
[22] Solomon W M *et al* 2006 Experimental test of the neoclassical theory of impurity poloidal rotation in tokamaks *Phys. Plasmas* **13** 056116
[23] Grierson B, Burrell K, Solomon W, Budny R and Candy J 2013 Collisionality scaling of main-ion toroidal and poloidal rotation in low torque DIII-d plasmas *Nucl. Fusion* **53** 063010
[24] Kim J, Burrell K H, Gohil P, Groebner R J, Kim Y-B, St John H E, Seraydarian R P and Wade M R 1994 Rotation characteristics of main ions and impurity ions in H-mode tokamak plasma *Phys. Rev. Lett.* **72** 2199–202
[25] Meister H, Kallenbach A, Peeters A G, Kendl A, Hobirk J and Pinches S D 2001 Measurement of poloidal flow, radial electric field and E×B shearing rates at ASDEX Upgrade *Nucl. Fusion* **41** 1633–44
[26] Chrystal C *et al* 2014 Testing neoclassical and turbulent effects on poloidal rotation in the core of DIII-D *Phys. Plasmas* **21** 072504
[27] Bortolon A, Duval B P, Pochelon A and Scarabosio A 2006 Observation of spontaneous toroidal rotation inversion in ohmically heated tokamak plasmas *Phys. Rev. Lett.* **97** 235003
[28] Duval B P, Bortolon A, Karpushov A, Pitts R A, Pochelon A and Scarabosio A 2007 Bulk plasma rotation in the TCV tokamak in the absence of external momentum input *Plasma Phys. Control. Fusion* **49** B195–209

[29] Rice J E *et al* 2011 Rotation reversal bifurcation and energy confinement saturation in tokamak ohmic *l*-mode plasmas *Phys. Rev. Lett.* **107** 265001

[30] Bugarya V I *et al* 1985 Measurements of plasma column rotation and potential in the TM-4 tokamak *Nucl. Fusion* **25** 1707

[31] Onchi T, Liu Y, Dreval M, McColl D, Elgriw S, Liu D, Asai T, Xiao C and Hirose A 2013 Effects of compact torus injection on toroidal flow in the STOR-M tokamak *Plasma Phys. Control. Fusion* **55** 035003

[32] Elgriw S, Liu Y, Hirose A and Xiao C 2016 Modification of plasma rotation with resonant magnetic perturbations in the STOR-M tokamak *Plasma Phys. Control. Fusion* **58** 045002

[33] Severo J H F, Nascimento I C, Tsypin V S and Galvão R M O 2003 Plasma residual rotation in the TCABR tokamak *Nucl. Fusion* **43** 1047

[34] Kim Y B, Diamond P H and Groebner R J 1991 Neoclassical poloidal and toroidal rotation in tokamaks *Phys. Fluids B: Plasma Phys.* **3** 2050–60

[35] Rice J E, Marmar E S, Bombarda F and Qu L 1997 X-ray observations of central toroidal rotation in ohmic Alcator C-Mod plasmas *Nucl. Fusion* **37** 421

[36] Suckewer S, Eubank H, Goldston R, McEnerney J, Sauthoff N and Towner H 1981 Toroidal plasma rotation in the PLT tokamak with neutral-beam injection *Nucl. Fusion* **21** 1301–9

[37] Yamamoto S, Maeno M and Sengoku S 1982 Transport studies in the JFT-2 tokamak *Proc. of the 9th Int. Conf. on Plasma Physics and Controlled Nuclear Fusion Research Held by the IAEA* vol 1 p 73

[38] Kostek C A and Marshall T C 1983 Observations of plasma rotation in the high beta Tokamak Torus II *Plasma Phys.* **25** 421–33

[39] Brau K, Bitter M, Goldston R J, Manos D, McGuire K and Suckewer S 1983 Plasma rotation in the PDX tokamak *Nucl. Fusion* **23** 1643–55

[40] Bugarya V *et al* 1985 Measurements of plasma column rotation and potential in the TM-4 tokamak *Nucl. Fusion* **25** 1707–17

[41] Isler R *et al* 1986 Rotation scalings and momentum confinement in neutral-beam-injected ISX-b plasmas *Nucl. Fusion* **26** 391–413

[42] Peebles W A, Brower D L and Philipona R 1990 Internal microturbulence studies on DIII-D, TEXT and TFTR *Proc. 13th Int. Conf. on Plasma Physics and Controlled Nuclear Fusion Research Held by the IAEA* vol 1 p 589

[43] Nave M F F *et al* 2012 JET intrinsic rotation studies in plasmas with a high normalized beta and varying toroidal field ripple *Plasma Phys. Control. Fusion* **54** 074006

[44] Duval B P, Joye B and Marchal B 1992 Behaviour of plasma rotation and radial electric field with density ramp rate in an ohmically heated tokamak *Nucl. Fusion* **32** 1405–19

[45] Severo J H F *et al* 2009 Temporal behaviour of toroidal rotation velocity in the TCABR tokamak *Nucl. Fusion* **49** 115026

[46] Rice J E *et al* 2007 Spontaneous toroidal rotation in Alcator C-Mod plasmas with no momentum input *Fusion Sci. Technol.* **51** 288–302

[47] Scarabosio A, Bortolon A, Duval B P, Karpushov A and Pochelon A 2006 Toroidal plasma rotation in the TCV tokamak *Plasma Phys. Control. Fusion* **48** 663–83

[48] Bernardo J *et al* 2015 Density impact on toroidal rotation in Tore Supra: experimental observations and theoretical investigation *Plasma Phys. Control. Fusion* **57** 035002

[49] Shukla G *et al* 2019 Observations of toroidal plasma rotation reversal in the Aditya-U tokamak *Nucl. Fusion* **59** 106049

[50] Parra F I, Nave M F F, Schekochihin A A, Giroud C, de Grassie J S, Severo J H F, de Vries P and Zastrow K D 2012 Scaling of spontaneous rotation with temperature and plasma current in tokamaks *Phys. Rev. Lett.* **108** 095001

[51] Severo J H F *et al* 2015 Investigation of rotation at the plasma edge in TCABR *Nucl. Fusion* **55** 093001

[52] Ronchi G 2010 Estudos de perfis de pressão no tokamak TCABR PhD Thesis Institute of Physics of the University of Sãido Paulo (IFUSP), São Paulo, Brazil (available at: https://teses.usp.br/teses/disponiveis/43/43134/tde-22022017-125032/en.php)

[53] Severo J H F, Nascimento I C, Kuznetov Y K, Tsypin V S, Galvão R M O and Tendler M 2007 Plasma rotation measurement in small tokamaks using an optical spectrometer and a single photomultiplier as detector *Rev. Sci. Instrum.* **78** 043509

[54] Puglia P G P, Elfimov A G, Andriati A V, Galvão R M O, Guimarães-Filho Z O, Ronchi G and Ruchko L F 2016 Mass number identification by Alfvén wave diagnostics in hydrogen and helium plasmas in TCABR *Phys. Lett.* A **380** 1189–92

[55] Rosenbluth M N, Hazeltine R D and Hinton F L 1972 Plasma transport in toroidal confinement systems *Phys. Fluids* **15** 116–40

[56] Hazeltine R D 1974 Rotation of a toroidally confined, collisional plasma *Phys. Fluids* **17** 961–8

[57] Hinton F L and Hazeltine R D 1976 Theory of plasma transport in toroidal confinement systems *Rev. Mod. Phys.* **48** 239–308

[58] Mikhailovskii A B and Tsypin V S 1982 Plasma transport drift equations *J. Exp. Theor. Phys.* **56** 75–9

[59] Tsypin V S, Severo J H F, Nascimento I C, Galvão R M O and Kuznetsov Y K 2001 Effect of plasma subsonic toroidal flows induced by Alfvèn waves on transport processes in the edge of elongated tokamaks *Braz. J. Phys.* **31** 34–41

[60] Severo J H F, Tsypin V S, Nascimento I C, Galvão R M O, Tendler M and Fagundes A N 2002 Neoclassical ion transport in the edge of axially-symmetric arbitrary cross-section tokamak with plasma subsonic toroidal flows *Braz. J. Phys.* **32** 13–9

[61] Tendler M 2010 Issues of electric fields in fusion devices *Plasma Fusion Res.* **5** S1004–7

[62] Rozhansky V and Tendler M 1996 Plasma rotation in tokamaks *Rev. Plasma Phys.* **19** 147

[63] Lao L L, John H S, Stambaugh R D, Kellman A G and Pfeiffer W 1985 Reconstruction of current profile parameters and plasma shapes in tokamaks *Nucl. Fusion* **25** 1611–22

[64] Doyle E J *et al* 2007 Chapter 2: plasma confinement and transport *Nucl. Fusion* **47** S18–127

[65] Severo J H F, Nascimento I C, Tsypin V S, Kuznetsov Y K, Saettone E A, Vannucci A, Galvão R M O, Tendler M and Mikhailovskii A B 2004 Magnetic islands and plasma rotation in the Tokamak Chauffage Alfvén Brésilien tokamak *Phys. Plasmas* **11** 846–8

[66] Rice J E *et al* 2007 Inter-machine comparison of intrinsic toroidal rotation in tokamaks *Nucl. Fusion* **47** 1618

[67] Claassen H A, Gerhauser H, Rogister A and Yarim C 2000 Neoclassical theory of rotation and electric field in high collisionality plasmas with steep gradients *Phys. Plasmas* **7** 3699–706

[68] Rogister A L 1999 A unified theory of transport barriers and of subneoclassical transport *Phys. Plasmas* **6** 200–13

[69] Fülöp T, Helander P and Catto P J 2002 Effect of poloidal density variation of neutral atoms on the tokamak edge *Phys. Rev. Lett.* **89** 225003

[70] Helander P, Fölöp T and Catto P J 2003 Controlling edge plasma rotation through poloidally localized refueling *Phys. Plasmas* **10** 4396–404

[71] Rozhansky V, Kaveeva E, Voskoboynikov S, Counsell G, Kirk A, Coster D and Schneider R 2005 Generation of

toroidal rotation by gas puff. Simulations of MAST experiments with B2SOLPS5.0 *J. Nucl. Mater.* **337** 291–5
[72] Rozhansky V 2013 Perpendicular currents and electric fields in fully and partially ionized magnetized plasma *Phys. Plasmas* **24** 101614
[73] Tendler M and Heifetz D 1987 Neutral particle kinetics in fusion devices *Fusion Technol.* **11** 289–310
[74] Harrison M F A 1986 *Atomic and Molecular Collisions in the Plasma Boundary* (Boston, MA: Springer US) pp 281–349
[75] Janev R, Langer W, Evans K and Post D 2012 *Elementary Processes in Hydrogen-Helium Plasmas: Cross Sections and Reaction Rate Coefficients Springer Series on Atomic, Optical and Plasma Physics* (Berlin: Springer)
[76] Cornelis J, Sporken R, van Oost G and Weynants R R 1994 Predicting the radial electric field imposed by externally driven radial currents in tokamaks *Nucl. Fusion* **34** 171–83